Journal of Materials Chemistry A

Accepted Manuscript

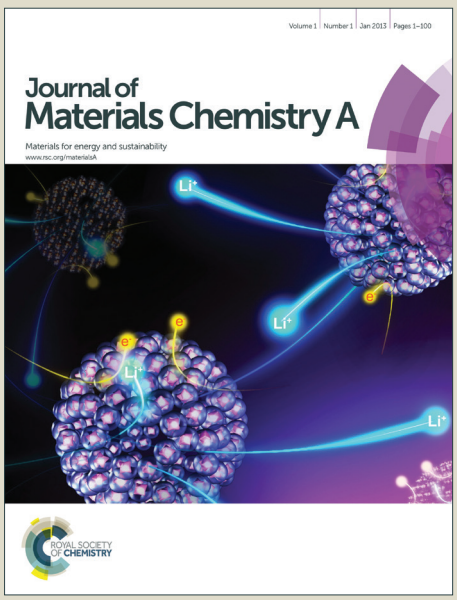

ROYAL SOCIETY OF CHEMISTRY

www.rsc.org/materialsA

Table of Contents Entry

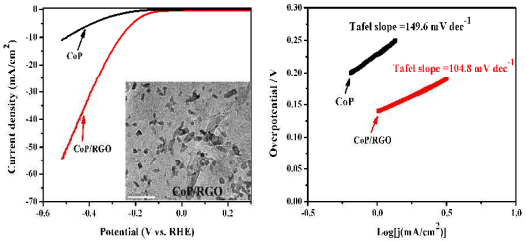

A novel CoP/RGO composite with excellent electrocatalytic activity toward HER was prepared through a facile two-step strategy.

Journal Name

RSCPublishing

ARTICLE

CoP nanoparticles deposited on reduced graphene oxide sheets as an active electrocatalyst for hydrogen evolution reaction

Cite this: DOI: 10.1039/x0xx00000x

Received 00th January 2012,
Accepted 00th January 2012

DOI: 10.1039/x0xx00000x

www.rsc.org/

Lianbo Ma,[a] Xiaoping Shen,*[a] Hu Zhou,[b,c] Guoxing Zhu,[a] Zhenyuan Ji[a] and Kangmin Chen[b]

A novel composite with CoP nanoparticles uniformly deposited on reduced graphene oxide (RGO) sheet is prepared through a facile two-step approach. The as-prepared CoP/RGO composite as electrocatalyst for hydrogen evolution reaction (HER) is investigated. It is found that the CoP/RGO composite shows an enhanced catalytic activity with a smaller Tafel slope (104.8 mV per decade), a much larger exchange current density (4.0×10^{-5} A/cm^2) and lower estimated HER activation energy (41.4 kJ/mol) than pure CoP. Besides, the CoP/RGO composite exhibits high stability in acidic solution, the HER catalytic activity of which shows no obvious degradation after 500 cycles. Such enhanced catalytic activity would stem from the abundance of catalytic active sites, the increase of electrochemically accessible surface area and significantly improved electrochemical conductivity of the CoP/RGO composite. The good catalytic activity demonstrates that the CoP/RGO composite could be a promising electrocatalyst in hydrogen production.

Introduction

Hydrogen is a promising alternative energy carrier that holds tremendous promise for clean and sustainable energy technology.[1,2] The conventional ways for the large scale production of hydrogen include natural gas reforming and gasification of coal and petroleum coke,[3,4] which involves the release of amounts of CO_2 and high energy consuming.[5] Hydrogen generation from electrochemical splitting of water has attracted increasing interests because it is the simplest way to produce hydrogen.[6-8] In order to increase the reaction rate and lower the overpotential, it is necessary to use an efficient hydrogen evolution reaction (HER) catalyst. Platinum group noble metals show high activity toward HER.[9,10] Unfortunately, their scarcity and high cost hindered their commercial application in large scale.[11,12] Thus, the exploration of highly active non-precious alternative catalysts has become a main research focus for the practical use of hydrogen.

The most extensively investigated non-precious HER catalysts include transition-metal complexes,[13,14] carbide[15,16] and non-precious metal alloys.[17] However, these HER catalysts usually suffer from poor HER activities.[18] Recently, it is well-accepted that the morphology and electrical conductivity of catalysts are the two key factors that influence their HER activity.[19] Taking these factors into account, carbon materials are ideal supports to improve the electrocatalytic activity owing to their unique physicochemical properties.[20-24] Especially, graphene, a one-atom-thick sheet of sp^2-bonded carbon atoms in a honeycomb crystal lattice, has been widely investigated recently as supports for HER catalysts.[25-28] The use of graphene sheets as the support material not only improves the conductivity of the hybrid catalysts, but also increases the dispersity of the active components due to their huge surface area and excellent electron conductivity. As a result, the graphene-based composite catalysts usually show enhanced catalytic activities.[27,28] For instance, Liao *et al.* reported the fabrication of MoS_2 nanoparticles deposited on graphene sheets, and the nanocomposite exhibits an enhanced electrocatalytic activity for the HER with a low overpotential and substantial apparent current densities as compared with pure MoS_2 nanoparticles.[25]

Recently, transition-metal phosphides including Ni_2P,[29] FeP[30], CoP[31,32], MoP[33], Cu_3P[34] and InP[35] have been demonstrated to be a new type of HER catalysts with high catalytic activity and low cost.[36] However, due to the complicated synthesis process and harsh fabrication conditions of transition-metal phosphides, there is a big difficulty in the combination of transition-metal phosphides and graphene. Up

to date, no reports have focused on transition-metal phosphides/graphene electrocatalysts. In this manuscript, a facile two-step approach was developed to synthesize the novel CoP/RGO nanocomposite with CoP nanoparticles uniformly deposited on reduced graphene oxide (RGO) sheets. The as-synthesized CoP/RGO composite as electrocatalyst ensures the effective utilization of both CoP and graphene, and exhibits an enhanced catalytic activity toward HER compared to pure CoP.

Experimental

Materials

Natural flake graphite with a particle size of 150 μm (99.9% purity) was purchased from Qingdao Guyu Graphite Co., Ltd. Nafion solution (5 wt%) was bought from Alfa Aesar. All of the other chemical reagents used in our experiments are of analytical grade, purchased from Sinopharm Chemical Reagent Co., Ltd, and used without further purification. Graphite oxide was prepared from natural flake graphite using a modified Hummers method.[37]

Synthesis of Co_3O_4/RGO composites

In a typical synthesis, 20 mg of the obtained graphite oxide was dispersed into a mixture solvent containing 24 mL of absolute ethanol and 0.5 mL of deionized water with ultrasonication for about 1 h to form a homogeneous graphene oxide (GO) dispersion. Subsequently, $Co(Ac)_2 \cdot 6H_2O$ was added into the above solution gradually under vigorous stirring. After stirring for about 3 h, 0.5 mL of $NH_3 \cdot H_2O$ (28 wt%) was introduced, and then the suspension was kept at 80 ℃ and stirred for 14 h. Then, the mixture was transferred to a stainless-steel autoclave and heated at 150 ℃ for 3 h. After the autoclave was cooled down to room temperature naturally, the product was collected by centrifugation, washed with absolute ethanol and deionized water for several times, and then dried in a vacuum oven at 60 ℃ for 24 h. The samples were designated as Co_3O_4/RGO-0.18, Co_3O_4/RGO-0.36, Co_3O_4/RGO-0.54 and Co_3O_4/RGO-0.72 for the feeding amount of 0.18, 0.36, 0.54 and 0.72 mmol of $Co(Ac)_2 \cdot 6H_2O$, respectively. Pure Co_3O_4 and bare RGO were prepared in the same way as the Co_3O_4/RGO-0.36 composite but without graphite oxide and $Co(Ac)_2 \cdot 6H_2O$ in the synthesis, respectively.

Synthesis of CoP/RGO composites

CoP/RGO composites were synthesized by using the as-synthesized Co_3O_4/RGO composites as precursors. Typically, 20 mg of Co_3O_4/RGO and 100 mg of sodium hypophosphite were mixed together and ground into a fine powder by using a mortar. Then the mixture was heated to 300 ℃ with a heating rate of 1 ℃/min and maintained at 300 ℃ for 2 h. After cooled to room temperature naturally, the product was collected, washed with deionized water and dried in a vacuum oven at 60 ℃ for 24 h. The final products were denoted as CoP/RGO-0.18, CoP/RGO-0.36, CoP/RGO-0.54, CoP/RGO-0.72 and CoP for the precursor of Co_3O_4/RGO-0.18, Co_3O_4/RGO-0.36, Co_3O_4/RGO-0.54, Co_3O_4/RGO-0.72 and Co_3O_4, respectively.

Instrumentation and measurements

The morphology and size of the as-prepared products were examined by scanning electron microscopy (SEM, JSM-6480) and transmission electron microscopy (TEM, JEM-2100). The phase structures were characterized using X-ray diffraction (XRD, Bruker D8 ADVANCE) with Cu-Kα radiation (λ = 1.5406 Å) at a scanning rate of 7° min^{-1}. The composition of the products was determined by energy-dispersive X-ray spectrometry (EDS). EDS was recorded with an energy dispersive spectrometer attached to the scanning electron microscope (JSM-6480). Raman scattering was performed on a DXR Raman spectrometer using a 532 nm laser source. The Brunauer-Emmett-Teller (BET) surface areas of the products were tested using a surface area and porosity analyzer (NDVA-2000e).

Electrochemical measurements

Electrochemical measurements were conducted on a typical three-electrode system using a CHI 760D electrochemical analyzer (Chen Hua Instruments, Shanghai China). Saturated calomel electrode (SCE) and Pt foil were used as the reference and counter electrodes, respectively. Glassy carbon electrode (GCE, 3 mm in diameter) coated with the as-prepared products (CoP/RGO composites, CoP, Co_3O_4/RGO composites, Co_3O_4 and RGO) were used as the working electrodes. As references, the electrochemical performances of commercial Pt/C and bare GCE were also conducted. Prior to the surface coating, the GCE was polished using 0.05 μm alumina powder, followed by sonication in absolute ethanol, and then allowed to dry at room temperature. In the fabrication of working electrode, catalyst ink was prepared by dispersing 5.0 mg of catalyst into a mixed solvent containing 0.98 mL of absolute ethanol and 20 μL of 5 wt% Nafion solution, and then the mixture was sonicated for about 30 min to form a homogeneous ink. After that, 4 μL of the catalyst ink was loaded onto GCE and dried at room temperature. Cyclic voltammetry (CV) and linear sweep voltammetry (LSV) were conducted in a 0.5 M H_2SO_4 aqueous solution. All the potentials reported in our work were calibrated with the reversible hydrogen electrode (RHE). In 0.5 M H_2SO_4 solution, the potential was converted to the RHE electrode according to the equation:[38] E (RHE) = E (SCE) + 0.281 V.

Results and discussion

Synthesis of the CoP/RGO composite

In this work, we developed a facile two-step strategy for the synthesis of CoP/RGO composite (Scheme 1). In the first step, graphite oxide was firstly dispersed in the mixed solvent (absolute ethanol and deionized water) to form GO sheets, which are highly negatively charged because of the ionization of the carboxylic acid and phenolic hydroxyl groups on their

edges and surface.[37] When the positively charged Co^{2+} ions were added, the electrostatic interaction between Co^{2+} and GO provides a strong driving force for the adsorption of Co^{2+} onto GO sheets. $NH_3 \cdot H_2O$ was then introduced to provide an alkaline environment, under which nucleation and growth of metal oxide/hydroxide species were highly selective on the functional groups of GO.[39] With the solvothermal treatment at 150 ℃, GO was converted to RGO in alkaline solution,[40] and meanwhile Co_3O_4 nanoparticles were formed on the RGO sheets. As a result, the Co_3O_4/RGO composite was obtained. In this solvothermal process, ethanol as the solvent allows the uniform distribution of the as-formed nanoparticles on RGO sheets, while the introduction of a little water ensures the formation of pure Co_3O_4 under the solvothermal condition. The optimal content of water was obtained from the control experiments, as shown in Fig. S1 in Supporting Information. In the second phase, the Co_3O_4/RGO composite was annealed at 300 ℃ in the presence of sodium hypophosphite. Under this condition, Co_3O_4 was reduced to Co nanoparticles by PH_3,[35,36] which was generated in situ from the thermal decomposition of NaH_2PO_2. Then the resulting Co catalyzed the decomposition of PH_3 into elemental P. Finally, the elemental P further reacted with Co to form CoP nanoparticles.[34,41] Consequently, the CoP/RGO composite with CoP nanoparticles decorated on RGO sheets was obtained. Considering the difficulty in integrating transition-metal phosphides with graphene, the effective two-step approach presented here could be extended to prepare other transition-metal phosphides/graphene composites through the phosphidation of the corresponding metal oxides/graphene precursors.

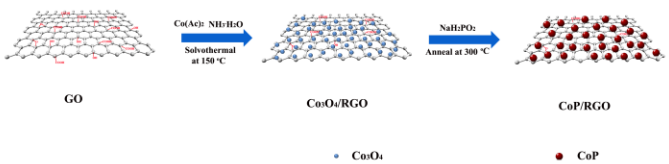

Scheme 1 Illustration of the formation process of CoP/RGO composites.

Structural and morphological characterization

The phase structures of the as-prepared samples were firstly determined by XRD technique. As shown in Fig. 1, the XRD pattern of graphite oxide shows a sharp diffraction peak at 2θ = 10.3 º, corresponding to the (001) reflection of graphite oxide.[42] However, the (001) peaks disappear in the XRD patterns of RGO, Co_3O_4/RGO-0.36 and CoP/RGO-0.36 composites, indicating that graphite oxide has been flaked to GO and then reduced into RGO in the synthesis.[43] Moreover, the XRD pattern of RGO shows a new broad diffraction peak at 2θ = 24.9 º, which can be ascribed to the (002) reflection of graphene sheets.[44] The peaks at 2θ values of 31.3 º, 36.8 º, 44.8 º, 59.3 ºand 65.2 ºin the XRD pattern of Co_3O_4/RGO-0.36 can be easily indexed to the (220), (311), (400), (511) and (440) planes of cubic Co_3O_4 (JCPDS No. 43-1003), respectively. After phosphidation, only the diffraction peaks of CoP are observed at 23.7 º, 32.0 º, 36.7 º, 45.1 º, 46.2 º, 48.4 º, 52.3 ºand 57.8 º, which can be indexed to the (101), (011), (102), (210), (112), (202), (103) and (301) planes of CoP (JCPDS No. 29-0497), respectively. It should be noted that the weak and broad peak at 2θ value of about 13º originates from the SiO_2 substrate used for XRD measurements, as shown in Fig. S2 (see Supporting Information). For comparison, the XRD patterns of pure Co_3O_4 and CoP were also investigated (Fig. S3, see Supporting Information), further confirming the successful preparation of Co_3O_4 and CoP under the current experimental conditions. The EDS spectrum of CoP/RGO-0.36 is presented in Fig. S4 (see Supporting Information), in which carbon, oxygen, cobalt and phosphorus elements were detected. The carbon element comes from RGO, while the oxygen element originates from the residual oxygen-containing groups on RGO sheets. The atomic ratio of Co to P was found to be almost 1 : 1, which is well consistent with that of CoP.

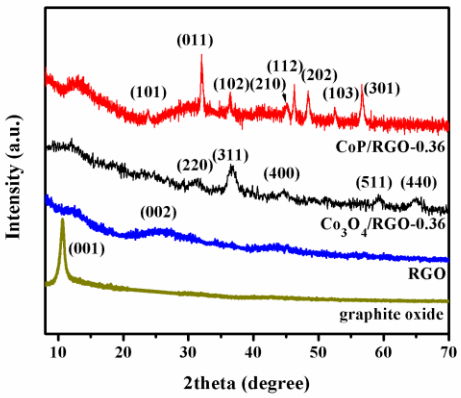

Fig. 1 XRD patterns of graphite oxide, RGO, Co_3O_4/RGO-0.36 and CoP/RGO-0.36 composites.

The morphology, size and microstructure of the as-prepared samples were investigated by SEM, TEM and high-resolution TEM (HRTEM). The typical TEM image of Co_3O_4/RGO-0.36 composite is presented in Fig. 2a. Graphene edges can be observed from the image, as marked with black arrow, indicating the presence of RGO. Monodispersed Co_3O_4 nanoparticles are exclusively deposited on RGO sheets with homogeneous distribution. The nanoparticles can act as "spacer", preventing the RGO sheets from aggregation and restacking. The average size of the nanoparticles is 4.1 nm (inset of Fig. 2a), which could provide more active sites for HER.[45] The HRTEM image (Fig. 2b) shows two different kinds of lattice fringes, in which the lattice spacings of 0.24 and 0.20 nm can be attributed to the (311) and (400) planes of Co_3O_4, respectively.

After phosphidation, the integration between the nanoparticles and RGO sheets is preserved. However, compared to the original Co_3O_4 nanoparticles, the formed CoP nanoparticles show much irregular non-spherical shape (Fig. 2c-e) and bigger particle sizes (average size about 7.5 nm, inset of Fig. 2c). HRTEM image (Fig. 2f) of CoP/RGO-0.36

composite reveals the good crystallinity of CoP nanoparticles. The lattice fringes with spacings of 0.28 and 0.19 nm match well with the (011) and (211) planes of CoP, respectively. TEM images of other Co_3O_4/RGO and CoP/RGO composites are presented in Fig. S5 (see Supporting Information), these composites show the similar characteristics as observed from Co_3O_4/RGO-0.36 and CoP/RGO-0.36, respectively. This indicates that the present approach is highly effective for the fabrication of CoP/RGO composites. For comparison, SEM images of pure Co_3O_4 and CoP are presented in Fig. S6 (see Supporting Information), from which the particle sizes are observed in the range of 1-3 μm. This demonstrates that RGO plays a key role for the generation of small-sized particles.

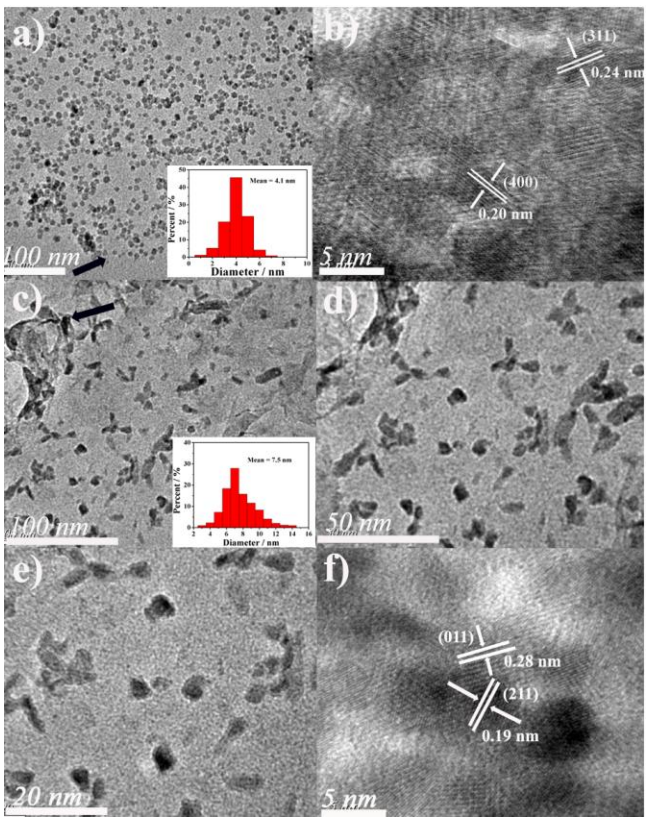

Fig. 2 (a) TEM image and (b) HRTEM image of Co_3O_4/RGO-0.36 composite; (c-e) TEM images and (f) HRTEM image of CoP/RGO-0.36 composite. The insets of (a) and (c) show the size distribution diagrams of Co_3O_4 and CoP nanoparticles, respectively.

Raman spectroscopy is a widely used tool to characterize the structural properties of graphene-based materials, such as disorder and defect structures.[46,47] The Raman spectra of graphite oxide, RGO, Co_3O_4/RGO-0.36 and CoP/RGO-0.36 are shown in Fig. 3. All of the spectra display two prominent peaks, corresponding to the well-documented D and G bands. The D band, at approximately 1356 cm^{-1}, is associated with structural defects and disorders that break the symmetry and selection rule, while the G band, observed at 1598 cm^{-1}, is usually assigned to the E_{2g} phonon of C sp^2 domains.[48,49] The integrated intensity ratio of D to G band (I_D/I_G) is usually used as a measure of structural defects and disorders in graphitic structures.[50] The I_D/I_G values of graphite oxide, RGO, Co_3O_4/RGO-0.36 and CoP/RGO-0.36 composite are *ca.* 1.86, 1.97, 2.17 and 2.24, respectively. Compared with graphite oxide, an increased I_D/I_G value was observed for bare RGO, demonstrating that more disorder carbon structure was produced after the exfoliation and reduction of graphite oxide.[51] For Co_3O_4/RGO-0.36 composite, the further increased I_D/I_G value as compared with bare RGO can be ascribed to the Co_3O_4 nanoparticles on RGO sheets, which can stress its surface and induce more disorders.[52] The Raman peaks at 460, 510 and 670 cm^{-1} can be attributed to the E_g, F_{2g} and A_{1g} modes of Co_3O_4, respectively.[53,54] After phosphidation, the higher I_D/I_G value of CoP/RGO-0.36 as compared with Co_3O_4/RGO-0.36 can be attributed to the increased structural defects and disorders caused during the thermal annealing process. In addition, no Raman peaks from CoP nanoparticles is observed in the Raman spectrum of CoP/RGO-0.36, which is well consistent with the previous report.[55]

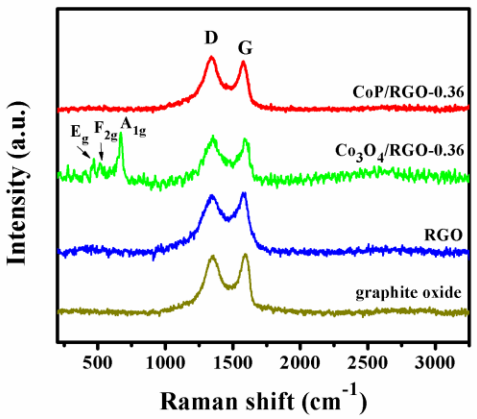

Fig. 3 Raman spectra of graphite oxide, RGO, Co_3O_4/RGO-0.36 and CoP/RGO-0.36 composites.

Electrocatalytic activities of the as-prepared composites toward HER

To examine their electrocatalytic activities toward HER, CoP/RGO composites, pure CoP and RGO were deposited on GCEs with a loading density of 0.29 mg/cm^2. The HER activities were then measured in 0.5 M H_2SO_4 solution using a typical three-electrode setup. Before the LSV measurements, CV was performed to stabilize or saturate the electrocatalysts in the electrolyte, the results are shown in Fig. S7 (see Supporting Information). Fig. 4a shows the LSV polarization curves of CoP/RGO composites, pure CoP and bare RGO electrodes at the scan rate of 2 mV s^{-1} at 298 K. As control experiments, the electrochemical performances of commercial Pt/C electrode and bare GCE were also investigated for comparison. Obviously, the Pt/C electrode shows the lowest overpotential, indicating the highest electrocatalytic activity for HER,[26] while the bare GCE electrode shows no electroactivity. The overpotentials for CoP/RGO composites catalysts are smaller

than that of pure CoP particles and bare RGO, demonstrating that both pure CoP particles and bare RGO electrodes exhibit inferior HER activities as compared to CoP/RGO composites catalysts. The improved electrochemical performance of CoP/RGO composites can be attributed to the chemical and electronic coupling between CoP nanoparticles and RGO sheets.[56] On the one hand, graphene can act as an ideal conductivity additive due to its unique electrical properties, and the conductivity of CoP/RGO could be significantly improved by incorporating RGO sheets (as proved by the Nyquist plots in Fig. S8, see Supporting Information). On the other hand, RGO provided a large surface area (Fig. S9, see Supporting Information) for the well dispersion of CoP nanoparticles, forming much smaller CoP nanoparticles as compared with the pure CoP product. The smaller CoP particles in the hybrid favor the exposure of more active sites for the HER.[57] This result further proves the advantages of RGO sheets as a direct substrate for the growth of catalyst active components, offering excellent electronic behavior and increased electrical conductivity. Thus, much faster electron transfer of the CoP/RGO catalysts is one of the key factors contributing to the greatly enhanced catalytic activity toward HER.[58]

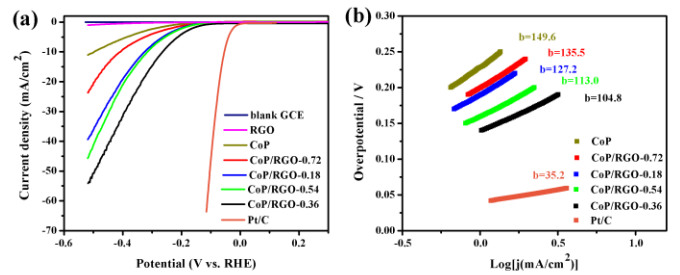

Fig. 4 (a) LSV polarization curves for CoP/RGO, pure CoP, RGO, bare GCE and Pt/C electrodes at the scan rate of 2 mV s^{-1} at 298 K, and (b) the corresponding Tafel plots of CoP/RGO composites, pure CoP and Pt/C catalysts.

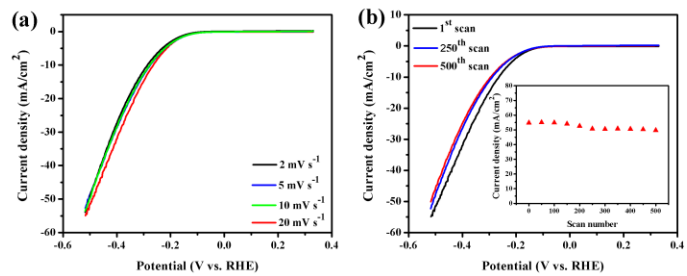

Fig. 5 (a) LSV polarization curves of CoP/RGO-0.36 electrode at various scan rates, (b) LSV polarization curves of CoP/RGO-0.36 electrode at the different scan numbers. The inset of (b) shows the cycling stability of CoP/RGO-0.36 electrode within 500 scanning cycles.

In addition, it is notable that the loading amount of CoP nanoparticles on RGO sheets also has an obvious influence on the electrocatalytic activities of CoP/RGO catalysts. With the increasing loading amount, the catalytic activity increases at first and then decrease. CoP/RGO-0.36 catalyst exhibits the highest electrocatalytic activity toward HER among these CoP/RGO catalysts. The first increment in electrocatalytic activity of CoP/RGO composites is attributed to the increased content of CoP participating in the electrochemical reaction, while the following decrement in electrocatalytic activity can be mainly ascribed to the decrease of the conductivity of CoP/RGO composites. This result demonstrates that the incorporation of RGO as well as its contents in the final composites greatly influences the electron transport and reaction kinetics during the HER.[23] For comparison, the catalytic activities of Co_3O_4/RGO composites and Co_3O_4 electrodes were also investigated, and the results are shown in Fig. S10 (see Supporting Information). The catalytic activities of Co_3O_4/RGO and Co_3O_4 electrodes are much lower than those of CoP/RGO and CoP electrodes.

The Tafel plots for CoP/RGO composites, pure CoP and Pt/C electrocatalysts are shown in Fig. 4b. The linear portions of the Tafel plots were fitted by the Tafel equation ($\eta = b\log j + a$, where j is the current density and b is the Tafel slope), yielding Tafel slopes of approximately 104.8 and 149.6 mV per decade for CoP/RGO-0.36 composite and pure CoP, respectively. The exchange current densities (j_0) for CoP/RGO-0.36 and pure CoP electrodes are *ca.* 4.0×10^{-5} and 6.3×10^{-7} A/cm^2, respectively. These results demonstrate that the CoP/RGO-0.36 composite possesses much higher catalytic activity toward HER than the pure CoP catalyst.[59] However, in comparison with that of Pt/C electrocatalyst (35.2 mV per decade), the electrocatalytic activity of CoP/RGO electrocatalysts is still relatively low.

The LSV polarization curves of CoP/RGO-0.36 composite at various scan rates are shown in Fig. 5a. It can be seen that the current density increases slightly, from 54.3 to 54.9 mA/cm^2, with increasing scan rate from 2 to 20 mV s^{-1} at potential of -0.5 V *vs* RHE, revealing that the catalytic activity of CoP/RGO composites toward HER is less affected by scan rates.[60] The catalytic stability of the CoP/RGO composite was also assessed. Fig. 5b shows the LSV polarization curves of CoP/RGO-0.36 at different scan numbers with scan rate of 20 mV s^{-1}. After 500 cycles, the catalyst shows a similar polarization curve. As shown in the inset of Fig. 6b, only a very slight decay of current density (from 54.9 to 50.1 mA/cm^2) was detected after the 500 cycles, indicating that the CoP/RGO composite catalyst possesses good long-term stability. The catalyst poisoning and/or the delamination of the catalyst from the electrode may contribute to the slight loss in catalytic activity.[59,61]

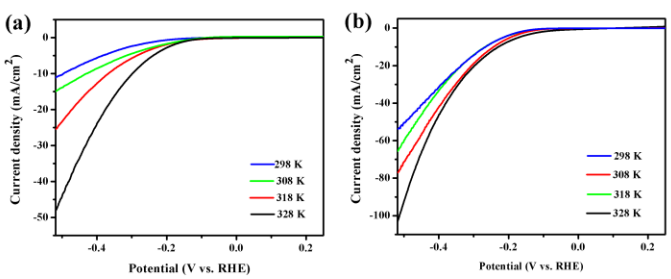

Fig. 6 LSV polarization curves of (a) pure CoP and (b) CoP/RGO-0.36 electrodes at different temperatures.

In order to investigate the influence of electrolytic temperature on the catalytic activity of CoP/RGO catalyst toward HER, LSV polarization measurements of CoP/RGO-0.36 composite and pure CoP catalysts at different temperatures were performed. Fig. 6 presents the corresponding LSV polarization curves at the temperature of 298, 308, 318 and 328 K. It can be seen that the overpotentials of both electrodes decrease with the increasing temperature from 298 to 328 K, and on the contrary, their current densities increase with the increase of the temperature. The kinetic parameters of the two electrodes at various temperatures estimated from the Tafel plots are summarized in Table S1 (see Supporting Information). It is obvious that the j_0 values of the two electrodes increase with the increase of the electrolytic temperature, suggesting that the catalytic activities of these two electrodes toward HER can be significantly enhanced through improving the electrolytic temperature. The values of active energy (E_a) for HER which is usually used to evaluate the intrinsic catalytic activity of the electrode can be calculated from Arrhenius curves of the electrode.[62-64] Based on the regression lines shown in Fig. 7, the E_a values for CoP/RGO-0.36 and pure CoP are determined to be *ca.* 41.4 and 82.7 kJ/mol, respectively. Compared with pure CoP, the CoP/RGO-0.36 catalyst has a much lower E_a value for HER, suggesting the higher HER activity.[5] The much lower E_a value of the CoP/RGO-0.36 catalyst can be attributed to the presence of a conductive graphene network, which can promote the electron transfer during the LSV polarization measurements.[38]

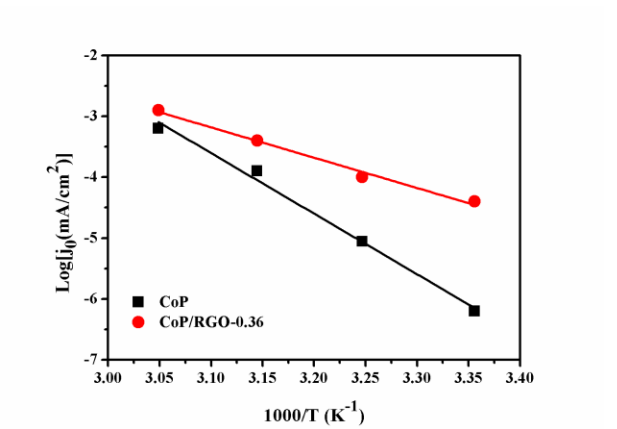

Fig. 7 Arrhenius curves of pure CoP and CoP/RGO-0.36 electrodes.

Conclusions

In summary, a novel composite with CoP nanoparticles deposited on RGO sheets was prepared through a facile two-step method. The CoP nanoparticles with an average size of *ca.* 7.5 nm were uniformly distributed on RGO sheets. The CoP/RGO composites exhibit a greatly enhanced catalytic activity toward HER as compared with pure CoP. Especially, the CoP/RGO composite exhibited a smaller Tafel slope than CoP, and the j_0 value of the CoP/RGO-0.36 catalyst was *ca.* 63.5 times higher than that of pure CoP catalyst. The enhanced catalytic activity of CoP/RGO catalysts can be attributed to the presence of RGO sheets, which increase the composite electrical conductivity and provide more active sites for HER. Moreover, the loading amount of CoP nanoparticles on RGO sheets is also crucial for the optimal catalytic activity. This study provides a simple approach for preparing transition-metal phosphides/graphene composite electrocatalysts, and the outstanding catalytic activity toward HER make CoP/RGO composites the promising catalysts in practical hydrogen production.

Acknowledgements

The authors are grateful for financial support from National Nature Science Foundation of China (No. 51272094), Specialized Research Fund for the Doctoral Program of Higher Education of China (No. 20123227110018), China Postdoctoral Science Foundation (2014M561578) and Jiangsu Planned Projects for Postdoctoral Research Funds (1401109C).

Notes and references

[a] School of Chemistry and Chemical Engineering, Jiangsu University, Zhenjiang 212013, P. R. China, Fax: (+86)511-88791800; Tel: (+86)511-88791800; E-mail: xiaopingshen@163.com
[b] School of Material Science and Engineering, Jiangsu University, Zhenjiang 212003, P. R. China
[c] School of Material Science and Engineering, Jiangsu University of Science and Technology, Zhenjiang 212003, P. R. China

1 M. S. Dresselhaus and I. L. Thomas, *Nature*, 2001, **414**, 332-337.
2 N. S. Lewis and D. G. Nocera, *Proc. Natl. Acad. Sci. USA*, 2006, **103**, 15729-15735.
3 M. A. Rosen and D. S. Scott, *Int. J. Hydrogen Energy*, 1998, **23**, 653-659.
4 D. Trommer, F. Noembrini, A. Fasciana, D. Rodriguez, A. Morales, M. Romero and A. Steinfeid, *Int. J. Hydrogen Energy*, 2005, **30**(6), 605-618.
5 T. W. Lin, C. J. Liu and C. S. Dai, *Appl. Catal. B*, 2014, **154**, 213-220.
6 M. G. Ealter, E. L. Warren, J. R. McKone, S. W. Boettcher, Q. Mi, E. A. Santori and N. S. Lewis, *Chem. Rev.*, 2010, **110**, 6446-6473.
7 D. Merki, H. Vrubel, L. Rovelli, S. Fierro and X. Hu, *Chem. Sci.* 2012, **3**, 2515-2525.
8 P. Ge, M. D. Scanlon, P. Peljo, X. Bian, H. Vubrel, A. Oneill, J. N. Coleman, M. Cantoni, X. Hu, K. Kontturi, B. Liu and H. H. Girault, *Chem. Commun.*, 2012, **48**, 6484-6486.
9 P. Millet, F. Andolfatto and R. Durand, *Int. J. Hydrogen Energy*, 1996, **21**, 87-93.
10 H. B. Gray, *Nat. Chem.*, 2009, **1**, 7-7.
11 T. Y. Wang, J. Q. Zhuo, K. Z. Du, B. B. Chen, Z. W. Zhu, Y. H. Shao and M. X. Li, *Adv. Mater.*, 2014, **26**, 3761-3766.
12 J. F. Xie, J. J. Zhang, S. Li, F. B. Grote, X. D. Zhang, H. Zhang, R. X. Wang, Y. Lei, B. C. Pan and Y. Xie, *J. Am. Chem. Soc.*, 2013, **135**, 17881-17888.
13 D. J. Evans and C. J. Pickett, *Chem. Soc. Rev.*, 2003, **32**, 268-275.
14 A. Volbeda and J. C. Fontecilla-Camps, *Dalton Trans.*, 2003, 4030-4038.

15 H. Vrubel and X. Hu, *Angew. Chem. Int. Ed.*, 2012, **51**, 12703-12706.
16 F. Harnisch, G. Sievers and U. Schroder, *Appl. Catal. B*, 2009, **89**, 455-458.
17 J. R. McKone, B. F. Sadtler, C. A. Werlang, N. S. Lewis and H. B. Gray, *ACS Catal.*, 2013, **3**, 166-169.
18 P. Xiao, Y. Yan, X. M. Ge, Z. L. Liu, J. Y. Wang and X. Wang, *Appl. Catal. B*, 2014, **154**, 232-237.
19 T. F. Jaramillo, K. P. Jorgensen, J. Bonde, J. H. Nielsen, S. Horch, I. Chorkendorff, *Science*, 2007, **317**, 100-102.
20 Y. Li, H. Wang, L. Xie, Y. Liang, G. Hong and H. Dai, *J. Am. Chem. Soc.*, 2011, **133**, 7296-7299.
21 T. W. Lin, C. J. Liu and J. Y. Lin, *Appl. Catal. B*, 2013, **134**, 75-82.
22 E. G. S. Firmiano, M. A. L. Cordeiro, A. C. Rabelo, C. J. Dalmaschio, A. N. Pinheiro, E. C. Pereira and E. R. Leite, *Chem. Commun.*, 2012, **48**, 7687-7689.
23 Y. Yan, B. Xia, X. Qi, H. Wang, R. Xu, J. Y. Wang, H. Zhang and X. Wang, *Chem. Commun.*, 2012, **49**, 4884-4886.
24 Y. Yan, X. Ge, Z. Liu, J. Y. Wang, J. M. Lee and X. Wang, *Nanoscale*, 2013, **5**, 7768-7771.
25 L. Liao, J. Zhu, X. J. Bian, L. N. Zhu, M. D. Scanlon, H. H. Girault and B. H. Liu, *Adv. Funct. Mater.*, 2013, **23**, 5326-5333.
26 H. Tang, K. P. Dou, C. C. Kaun, Q. Kuang and S. H. Yang, *J. Mater. Chem. A*, 2014, **2**, 360-364.
27 Y. Liang, Y. Li, H. Wang and H. Dai, *J. Am. Chem. Soc.*, 2013, **135**, 2013-2036.
28 H. Huang and X. Wang, *J. Mater. Chem. A*, 2014, **2**, 6266-6291.
29 E. J. Popczun, J. R. McKone, C. G. Read, A. J. Biacchi, A. M. Wiltrout, N. S. Lewis and R. E. Schaak, *J. Am. Chem. Soc.*, 2013, **135**, 9267-9270.
30 Y. Xu, R. Wu, J. F. Zhang, Y. M. Shi and B. Zhang, *Chem. Commun.*, 2013, **49**, 6656-6658.
31 H. F. Du, Q. Liu, N. Y. Cheng, A. M. Asiri, X. P. Sun and C. M. Li, *J. Mater. Chem. A*, 2014, **2**, 14812-14816.
32 S. Gu, H. F. Du, A. M. Asiri, X. P. Sun, C. M. Li, *Phys. Chem. Chem. Phys.*, 2014, **16**, 16909-16913.
33 P. Xiao, M. A. Sk, L. Thia, X. M. Ge, R. J. Lim, J. Y. Wang, K. H. Lim and X. Wang, *Energy & Environ. Sci.*, 2014, **7**, 2624-2629.
34 J. Q. Tian, Q. Liu, N. Y. Cheng, A. M. Asiri and X. P. Sun, *Angew. Chem. Int. Ed.*, 2014, **53**, 9577-9581.
35 Q. Guan and W. Li, *J. Catal.*, 2010, **271**, 413-415.
36 S. T. Oyama, T. Gott, H. Zhao and Y. K. Lee, *Catal. Today*, 2009, **143**, 94-107.
37 Z. Y. Ji, X. P. Shen, G. X. Zhu, H. Zhou, A. H. Yuan, *J. Mater. Chem.*, 2012, **22**, 3471-3477.
38 X. L. Zheng, J. B. Xu, K. Y. Yan, H. Wang, Z. L. Wang and S. H. Yang, *Chem. Mater.*, 2014, **26**, 2344-2353.
39 Y. Y. Liang, H. L. Wang, P. Diao, W. Chang, G. S. Hong, Y. G. Li, M. Gong, L. M. Xie, J. G. Zhou, J. Wang, T. Z. Regier, F. Wei and H. J. Dai, *J. Am. Chem. Soc.*, 2012, **134**, 15849-15857.
40 Z. Wang, X. Zhang, Y. Li, Z. T. Liu and Z. P. Hao, *J. Mater. Chem. A*, 2013, **1**, 6393-6399.
41 A. E. Henkes, Y. Vasquez and R. E. Schaak, J. Am. Chem. Soc., 2007, **129**, 1896-1897.
42 L. B. Ma, X. P. Shen, G. X. Zhu, Z. Y. Ji and H. Zhou, *Carbon*, 2014, **77**, 255-265.
43 L. B. Ma, X. P. Shen, Z. Y. Ji, G. X. Zhu and H. Zhou, *Chem. Eng. J.*, 2014, **252**, 95-103.
44 Z. Y. Ji, X. P. Shen, J. L. Yang, G. X. Zhu and K. M. Chen, *Appl. Catal. B*, 2014, **144**, 454-461.
45 D. H. Ha, L. M. Moreau, C. R. Bealing, H. T. Zhang, R. G. Hennig and R. D. Robinson, *J. Mater. Chem.*, 2011, **21**, 11498-11510.
46 A. P. A. Raju, A. Lewis, B. Derby, R. J. Young, I. A. Kinloch, R. Zan and K. S. Novoselov, *Adv. Funct. Mater.*, 2014, **24**, 2865-2874.
47 X. H. Li, W. C. H. Choy, X. G. Ren, D. Zhang and H. F. Lu, *Adv. Funct. Mater.*, 2014, **24**, 3114-3122.
48 F. Tuinstra and J. L. Koenig, *J. Chem. Phys.*, 1970, **53**, 1126.
49 D. Graf, F. Molitor, K. Ensslin, C. Stampfer, A. Jungen, C. Hierold and L. Wirtz, *Nano Lett.*, 2007, **7**, 238-242.
50 S. Stankovich, D. A. Dikin, R. D. Piner, K. A. Kohlhaas, A. Kleinhammes, Y. Jia, Y. Wu, S. T. Nguyen and R. S. Ruoff, *Carbon*, 2007, **45**, 1558-1565.
51 C. Xu, X. Wang, J. W. Zhu, *J. Phys. Chem. C*, 2008, **112**, 19841-19845.
52 Y. Y. Wen, H. M. Ding and Y. K. Shan, *Nanoscale*, 2011, **3**, 4411-4417.
53 P. B. Liu, Y. Huang and X. Sun, *ACS Appl. Mater. Interfaces*, 2013, **5**, 12355-12360.
54 J. H. Jiang, W. D. Shi, S. Y. Song, Q. L. Hao, W. Q. Fan, X. F. Xia, X. Zhang, Q. Wang, C. B. Liu and D. Yan, *J. Power Sources*, 2014, **248**, 1281-1289.
55 C. J. Carmalt, D. E. Morrison and I. P. Parkin, *Polyhedron*, 2000, **19**, 829-833.
56 Y. D. Ma, Y. Dai, M. Guo, C. W. Niu and B. B. Huang, *Nanoscale*, 2011, **3**, 3883-3887.
57 K. P. de Jong, *Curr. Opin. Solid. State Mater. Sci.*, 1999, **4**, 55-62.
58 K. Chang and W. X. Chen, *Chem. Commun.*, 2011, **47**, 4252-4254.
59 J. Xie, H. Zhang, S. Li, R. Wang, X. Sun, M. Zhou, J. Zhou, X. W. Lou and Y. Xie, *Adv. Mater.*, 2013, **25**, 5807-5813.
60 C. B. Ma, X. Y. Qi, B. Chen, S. Y. Bao, Z. Y. Yin, X. J. Wu, Z. M. Luo, J. Wei, H. L. Zhang and H. Zhang, *Nanoscale*, 2014, **6**, 5624-5629.
61 J. Benck, Z. B. Chen, L. Y. Kuritzky, A. J. Forman and T. F. Jaramillo, *ACS Catal.*, 2012, **2**, 1916-1923.
62 M. J. Giz, S. C. Bento and E. R. Gonzalez, *Int. J. Hydrogen Energy*, 2000, **25**, 621-626.
63 Z. Shan, Y. Liu, Z. Chen, G. Warrender and J. Tian, *Int. J. Hydrogen Energy*, 2008, **33**, 28-33.
64 B. Liu, J. B. He, Y. J. Chen and N. Deng, *Int. J. Hydrogen Energy*, 2013, **38**, 3130-3136.